3D Rainbow Beam Design for Fast Beam Training with True-Time-Delay Arrays in Wideband Millimeter-Wave Systems

Aditya Wadaskar, Veljko Boljanovic, Han Yan, and Danijela Cabric
Department of Electrical and Computer Engineering, University of California, Los Angeles
Email: adityaw@ucla.edu, vboljanovic@ucla.edu, yhaddint@ucla.edu, danijela@ee.ucla.edu

(Invited Paper)

2021 55th Asilomar Conference on Signals, Systems, and Computers | 978-1-6654-5828-3/21/$31.00 ©2021 IEEE | DOI: 10.1109/IEEECONF53345.2021.9723402

***Abstract*—True-time-delay (TTD) arrays can implement frequency-dependent rainbow beams and enable fast beam alignment in wideband millimeter-wave (mmWave) systems. In this paper, we consider the design of 3D rainbow beams for TTD-based beam training using planar arrays which are of great interest in practical deployments. We firstly design a codebook for a rectangular TTD array to realize beams that scan the entire 3D sphere using one Orthogonal Frequency Division Multiplexing (OFDM) symbol. Specifically, we determine a proper configuration of delays in TTD circuits and the minimum number of OFDM subcarriers that guarantee that all angular directions are probed at once using frequency-dependent beams. We then propose a frequency-domain power-based beam training algorithm to estimate the dominant propagation direction in terms of the azimuth and elevation angles. Lastly, we numerically evaluate the performance of the proposed algorithm in realistic mmWave channels as a function of the design and system parameters.**

I. Introduction

Millimeter-wave (mmWave) communication is a disruptive technology that relies on abundant spectrum to enable high data rates in the fifth generation (5G) of mobile networks. Due to the small wavelength, large antenna arrays with narrow beams can be used at both base stations and mobile terminals to enable directional communication and compensate for large propagation loss at mmWave frequencies. It is believed that in further evolution of 5G wireless networks, the carrier frequency and number of antenna elements will continue to grow, which makes the *beam training* challenging and time consuming when conventional phased arrays are used. Thus, novel beamforming techniques are necessary to facilitate the future evolution of mmWave communications. Recently, frequency-dependent beamforming (rainbow beams) emerged as a promising candidate for fast beam training [1], [2]. It can be enabled either by true-time-delay (TTD) based antenna arrays [3] or leaky wave antennas [4] in mmWave and sub-THz bands. Besides, for fast beam training, rainbow beams can also be leveraged for alignment-free multiple access schemes [5] and object tracking [6], [7]. In this work, we focus on fast 3D beam training using planar TTD arrays.

Design of 3D beam codebooks for planar phased arrays has been extensively studied in the literature [8]–[10]. In a codebook for planar phased arrays, each beam has independently designed phases. For an N-element array with M_{o} beams in the codebook, the number of designed phases is NM_{o}. The 3D beam codebook design for TTD arrays is much more challenging. In a TTD rainbow beam codebook design, there are limited degrees of freedom because the M_{o} beams pointing in different directions share the same set of N designed delays. To date, the TTD based codebook has been exclusively focused on linear arrays, where frequency dependent beam steering occurs in one plane of the spherical angular space. This work presents a 3D TTD-based rainbow beam codebook to enable fast beam training over the entire spherical angular space.

Our main contributions can be summarized as follows. Firstly, we characterize the 3D rainbow beam for a given set of delay taps by analyzing its center (pointing direction). It is shown that by introducing proper delays in all antenna elements, frequency dependent beams can simultaneously scan multiple angles in both the azimuth and elevation planes. Secondly, we propose sufficient conditions on the delay taps and the Orthogonal Frequency Division Multiplexing (OFDM) waveform design to guarantee that any arbitrary spherical angle pair in the field-of-view is covered by a rainbow beam with a desired beamforming gain. Lastly, we show that the proposed 3D rainbow beams can support beam training using a single OFDM pilot in realistic mmWave channels.

The paper is organized as follows. In Sec. II, we state the considered system model, including the array response and steering vectors of a planar TTD array architecture, and we formulate the problem of the 3D rainbow beam codebook design. The codebook design and analysis are presented in Sec. III. The results of numerical simulations are provided in Sec. IV. Sec. V concludes the paper and highlights the remaining research problems.

Notation: Scalars, vectors, and matrices are denoted by non-bold, bold lower-case, and bold upper-case letters, respectively. The (i,j)-th element of $\mathbf{A}$ is denoted by $[\mathbf{A}]_{i,j}$. Conjugate, transpose, Hermitian transpose, and pseudoinverse are denoted by $(.)^*$, $(.)^{\mathrm{T}}$, $(.)^{\mathrm{H}}$, and $(.)^{\dagger}$ respectively.

II. System Model

This section introduces the system model for wideband mmWave beam training and problem formulation.

A. TTD planar array

The TTD planar array has N_R antenna elements arranged in a rectangular array, with N_{az} and N_{el} elements along the

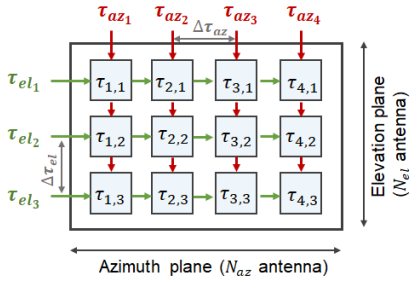

Fig. 1: TTD planar array layout with delay taps associated with each plane.

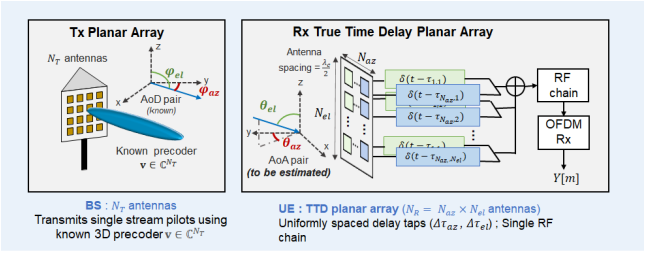

Fig. 2: Illustration of the transceiver and channel model.

azimuth and elevation planes, respectively, placed at half-wavelength $\lambda_c/2$ separation along each dimension. The TTD circuit block applies finite time delays $\tau_{az,n_{az}}$ and $\tau_{el,n_{el}}$ in each antenna branch in the azimuth and elevation planes, respectively, which enables frequency-dependent beam steering. In this work, we focus on uniformly spaced delays in both planes, i.e., $\tau_{az,n_{az}} = (n_{az}-1)\Delta\tau_{az}$ and $\tau_{el,n_{el}} = (n_{el}-1)\Delta\tau_{el}$, where $\Delta\tau_{az}$ and $\Delta\tau_{el}$ are the delay spacings between neighboring antenna elements in the azimuth and elevation planes respectively, as illustrated in Fig. 1. The total time delay in the (n_{az}, n_{el})-th antenna element $\tau_{n_{az},n_{el}}$ is given by $\tau_{n_{az},n_{el}} = \tau_{az,n_{az}} + \tau_{el,n_{el}}$.

B. System model for downlink TTD-based beam training

We consider a 5G-like single cell system where a base station (BS) is equipped with a planar phased array of N_{T} antennas as shown in Fig. 2. The user equipment (UE) is equipped with an analog planar TTD array receiver with N_{R} antennas, arranged in an $N_{az} \times N_{el}$ rectangular array. Beam training occurs in the downlink. The BS transmits a single OFDM symbol over a set of subcarriers, $\mathcal{M}$, where $M = |\mathcal{M}|$ subcarriers are loaded out of a total of M_{tot}. The m-th subcarrier is loaded with a pilot $X[m]$, $m \in \mathcal{M}$ which is precoded using a known frequency-flat beamforming vector $\mathbf{v}_{\mathrm{T}} \in \mathbb{C}^{N_{\mathrm{T}}}$. At the UE side, the received signal at the m-th subcarrier is combined using a frequency-dependent combiner $\mathbf{w}_{\mathrm{TTD}}[m]$.

The wideband frequency selective mmWave channel can be represented using the geometric multipath model. The frequency domain channel $\mathbf{H}[m] \in \mathbb{C}^{N_{\mathrm{R}} \times N_{\mathrm{T}}}$ at the m-th subcarrier is given as

$$\mathbf{H}[m] = \rho \sum_{l=1}^{L} \tilde{g}_l[m] \mathbf{a}_{\mathrm{R}}\left(\phi_{\mathrm{az},l}^{(\mathrm{R})}, \phi_{\mathrm{el},l}^{(\mathrm{R})}, f_m\right) \mathbf{a}_{\mathrm{T}}^{\mathrm{H}}\left(\phi_{\mathrm{az},l}^{(\mathrm{T})}, \phi_{\mathrm{el},l}^{(\mathrm{T})}, f_m\right) \tag{1}$$

where L is the number of multipath component (MPC), $\tilde{g}_l[m] = \sum_{i=0}^{M-1} e^{-j\frac{2\pi m}{M}} p_{\mathrm{c}}(iT_{\mathrm{s}} - \tau_l)$ is the complex gain of the l-th MPC, and function $p_{\mathrm{c}}(t)$ is the time domain response filter. The terms $\phi_{az,l}^{(\mathrm{T})}$, $\phi_{el,l}^{(\mathrm{T})}$, $\phi_{az,l}^{(\mathrm{R})}$, $\phi_{el,l}^{(\mathrm{R})}$ are the angle of departure (AoD) in the azimuth plane, AoD in the elevation plane, angle of arrival (AoA) in the azimuth plane, and AoA in the elevation plane of the l-th MPC. The terms $\lambda_{\mathrm{c}} = c/f_{\mathrm{c}}$ and c denote carrier wavelength and the speed of light respectively. The vectors $\mathbf{a}_{\mathrm{R}}\left(\phi_{\mathrm{az},l}^{(\mathrm{R})}, \phi_{\mathrm{el},l}^{(\mathrm{R})}, f_m\right)$ and $\mathbf{a}_{\mathrm{T}}\left(\phi_{\mathrm{az},l}^{(\mathrm{T})}, \phi_{\mathrm{el},l}^{(\mathrm{T})}, f_m\right)$ are the array responses at the receiver and transmitter respectively. The array response vector is given by the Kronecker product of the array responses in the azimuth and elevation planes as follows

$$\mathbf{a}_{\mathrm{R}}(\theta_{\mathrm{az}}, \theta_{\mathrm{el}}, f_m) = \mathbf{a}_{\mathrm{az}}(\theta_{\mathrm{az}}, \theta_{\mathrm{el}}, f_m) \otimes \mathbf{a}_{\mathrm{el}}(\theta_{\mathrm{el}}, f_m) \tag{2}$$

$$\begin{aligned} [\mathbf{a}_{\mathbf{az}}(\theta_{\mathrm{az}}, \theta_{\mathrm{el}}, f_m)]_{n_{\mathrm{az}}} &= e^{-j\pi(n_{\mathrm{az}}-1)\frac{f_m}{f_{\mathrm{c}}}\sin\theta_{\mathrm{az}}\sin\theta_{\mathrm{el}}} \\ [\mathbf{a}_{\mathrm{el}}(\theta_{\mathrm{el}}, f_m)]_{n_{\mathrm{el}}} &= e^{-j\pi(n_{\mathrm{el}}-1)\frac{f_m}{f_{\mathrm{c}}}\cos\theta_{\mathrm{el}}}. \end{aligned} \tag{3}$$

The frequency f_m corresponding to the m-th subcarrier is defined as

$$f_m = \begin{cases} f_{\mathrm{c}} + \frac{m}{M}\mathrm{BW}, & 0 \le m < \frac{M}{2} \\ f_{\mathrm{c}} - \frac{\mathrm{BW}}{2} + \frac{(m-\frac{M}{2})}{M}\mathrm{BW}, & \frac{M}{2} \le m < M \end{cases} \tag{4}$$

With the assumed system model, the received OFDM pilot at the m-th subcarrier after analog TTD combining is

$$Y[m] = \mathbf{w}_{\mathrm{TTD}}^{\mathrm{H}}[m]\mathbf{H}[m]\mathbf{v}_{\mathrm{T}}X[m] + N[m], \tag{5}$$

where $N[m] \sim \mathcal{CN}(0, \sigma_{\mathrm{n}}^2)$ is a sample of complex Gaussian noise at the m-th subcarrier.

C. TTD combiners and beamforming gain

The TTD combiner $\mathbf{w}_{\mathrm{TTD}}[m] \in \mathbb{C}^{N_R}$ is given by the Kronecker product of the frequency-dependent antenna weight vectors, $\mathbf{w}_{az}[m] \in \mathbb{C}^{N_{az}}$ and $\mathbf{w}_{el}[m] \in \mathbb{C}^{N_{el}}$, in the azimuth and elevation planes respectively.

$$\mathbf{w}_{\mathrm{TTD}}[m] = \mathbf{w}_{\mathrm{az}}[m] \otimes \mathbf{w}_{\mathrm{el}}[m] \tag{6}$$

where, $[\mathbf{w}_{\mathrm{az}}[m]]_{n_{az}} = \exp(j2\pi f_m(n_{az}-1)\Delta\tau_{\mathrm{az}})$ and $[\mathbf{w}_{\mathrm{el}}[m]]_{n_{el}} = \exp(j2\pi f_m(n_{el}-1)\Delta\tau_{\mathrm{el}})$.

The beamforming gain in the direction $(\theta_{az}, \theta_{el})$ for the beam centered at the frequency f_m is denoted by $G(\theta_{az}, \theta_{el}, f_m)$ and it can be expressed as the product of the beamforming gains in the azimuth $G_{az}(\Psi_{az})$ and elevation $G_{el}(\Psi_{el})$ as follows

$$\begin{aligned} G(\theta_{az}, \theta_{el}, f_m) &= \frac{1}{N_R}|\mathbf{w}_{\mathrm{TTD}}^{H}[m]\mathbf{a}_{\mathrm{R}}(\theta_{az}, \theta_{el}, f_m)|^2 \\ &= G_{az}(\theta_{az}, \theta_{el}, f_m)\, G_{el}(\theta_{el}, f_m) = G_{az}(\Psi_{az})\, G_{el}(\Psi_{el}) \end{aligned} \tag{7}$$

where $\Psi_{az} = 2f_m\Delta\tau_{az} + (f_m/f_c)\sin\theta_{az}\sin\theta_{el}$ and $\Psi_{el} = 2f_m\Delta\tau_{el} + (f_m/f_c)\cos\theta_{el}$ are the frequency-angle dependent arguments of the respective gain functions. The gains $G_{az}(\Psi_{az})$ and $G_{el}(\Psi_{el})$ are defined as

$$G_{az}(\Psi_{az}) = \frac{1}{N_{az}}\left|\frac{\sin\left[N_{az}\frac{\pi}{2}\Psi_{az}\right]}{\sin\left[\frac{\pi}{2}\Psi_{az}\right]}\right|^2 \tag{8}$$

$$G_{el}\left(\Psi_{el}\right)=\frac{1}{N_{el}}\left|\frac{\sin\left[N_{el}\frac{\pi}{2}\Psi_{el}\right]}{\sin\left[\frac{\pi}{2}\Psi_{el}\right]}\right|^{2}. \tag{9}$$

The gain $G_{az}\left(\Psi_{az}\right)$ achieves the peak gain of N_{az} at $\Psi_{az}=0$ and it is periodic in Ψ_{az} with the period 2 [11, Chapt 7.2.4]. Likewise, $G_{el}\left(\Psi_{el}\right)$ achieves the peak gain of N_{el} at $\Psi_{el}=0$ with the same period.

D. Problem formulation

1) 3D rainbow beam codebook design: The objective is to design the TTD planar array parameters, i.e. the delay tap spacings $\Delta\tau_{az}$ and $\Delta\tau_{el}$, and the number of subcarriers needed (M), to create frequency-dependent probing beams that can scan the entire 3D spherical angular space with sufficient beamforming gain. In other words, we need to find the limiting set of design parameters $\mathcal{S}$ that can achieve *full spherical coverage*, where any arbitrary direction $(\theta_{az},\theta_{el})$ sees at least one beam with beamforming gain $\geq(1-\epsilon)N_R$, where ϵ is the gain sounding factor.

$$\mathcal{S}=\{(\Delta\tau_{az},\Delta\tau_{el},M)\mid\min_{\theta_{\mathrm{az}},\theta_{\mathrm{el}}}\max_{m}G\left(\theta_{az},\theta_{el},f_m\right)\geq(1-\epsilon)N_{\mathrm{R}}$$
$$\forall\ (\theta_{az},\theta_{el})\in([-\pi/2,\pi/2],[0,\pi])$$

Spherical coverage efficiency: Realising the need for a metric to quantify spherical coverage, we define spherical coverage efficiency η_{cov} as the ratio of the continuous solid-angular region given by $\mathcal{A}=\left\{\left(\theta_{az},\theta_{el}\right)\middle|\max_{m}\ G\left(\theta_{az},\theta_{el},f_m\right)\ \geq\ \left(1-\epsilon\right)N_R\right\}$, and the total target solid-angular region of 2π, and is expressed as follows

$$\eta_{cov}=\frac{1}{2\pi}\iint_{(\theta_{az},\theta_{el})\in\mathcal{A}}\sin\theta_{el}d\theta_{el}d\theta_{az} \tag{10}$$

The spherical coverage efficiency computed on a discrete angular grid is the ratio of the cardinality of the set $\mathcal{A}^{grid}$ and the total number of grid elements.

We adopt a three step approach for our 3D rainbow beam codebook design problem to achieve full spherical coverage.

i Derive the beam-centres of frequency-dependent beams as a function of the delay tap spacings $\Delta\tau_{az}$ and $\Delta\tau_{el}$.
ii Define and express beam widths along the azimuth and elevation planes as a function of array dimensions and gain constraints in each plane.
iii Derive the conditions on $(\Delta\tau_{az},\Delta\tau_{el})$ and number of used subcarriers M to construct a codebook that achieves full (100%) spherical coverage.

2) 3D TTD codebook based fast beam training: Using the 3D beam codebook constructed with optimal design parameters in $\mathcal{S}$, we propose a frequency-domain power-based beam training algorithm to estimate the dominant AoA pair (azimuth and elevation angles) from the received pilots $Y[m]$ of a single OFDM training symbol.

III. 3D TTD BEAM CODEBOOK DESIGN

In this section, we propose the design of 3D beam codebook, i.e. the TTD planar array parameters $\Delta\tau_{az}$, $\Delta\tau_{el}$, and M, for a given array size. We first explain how the beam-centres are related to the subcarrier frequencies and delay spacings, by analyzing the beamforming gain expressions, in Sec. III-A. In Sec. III-B, we define beam widths along the azimuth and elevation planes as a function of number of antennas and gain constraints in the respective planes. We then discuss how the choice of delay tap spacings $\Delta\tau_{az}$ and $\Delta\tau_{el}$ affect rainbow beam trajectory and coverage in Sec. III-C. These insights lead us to derive the optimal delay spacings and number of training subcarriers that ensure full (100%) spherical coverage as defined in (10).

A. Frequency-dependent beam-centres

The pointing direction of the beam centred at frequency f_m is defined as the angle pair $\left(\theta^{\star}_{az,m},\theta^{\star}_{el,m}\right)$ that sees the maximum beamforming gain. That is, $\left\{\theta^{\star}_{\mathrm{az},m},\theta^{\star}_{\mathrm{el},m}\right\}=\left\{\left(\theta_{az},\theta_{el}\right)\middle|G\left(\theta_{az},\theta_{el},f_m\right)=N_R\right\}$. It follows from (7), (8) and (9) that the beam-centres must also individually maximise the azimuth and elevation beamforming gain functions. i.e. $G_{\mathrm{az}}\left(\theta^{\star}_{\mathrm{az},m},\theta^{\star}_{\mathrm{el},m},f_m\right)=N_{\mathrm{az}}\ ;\ G_{\mathrm{el}}\left(\theta^{\star}_{\mathrm{el},m},f_m\right)=N_{\mathrm{el}}$. Exploiting the periodicity of $G_{\mathrm{az}}\left(\Psi_{\mathrm{az}}\right)$ and $G_{\mathrm{el}}\left(\Psi_{\mathrm{el}}\right)$ with respect to the spectral-spatial arguments Ψ_{az} and Ψ_{el} (period $=2$), we obtain the analytical expressions for beam-centres in terms of azimuth and elevation angles by equating $\Psi_{\mathrm{az},m}$ and $\Psi_{\mathrm{el},m}$ to even integers $2z$, where $z\in\mathbb{Z}$. Since $G_{\mathrm{el}}\left(\Psi_{\mathrm{el}}\right)$ depends only on θ_{el}, we first compute $\theta^{\star}_{\mathrm{el},m}$ by solving (11). The beam-centre azimuth can then be found as $\theta^{\star}_{\mathrm{az},m}=\left\{\theta_{az}\middle|G\left(\theta_{az},\theta^{\star}_{\mathrm{el},m},f_m\right)=N_{\mathrm{az}}\right\}$. We compute $\theta^{*}_{\mathrm{az},m}$ by solving (12).

$$2f_m\Delta\tau_{el}+\frac{f_m}{f_c}\cos\theta_{el}=2z\ \ ;\ \ z\in\mathbb{Z} \tag{11}$$

$$2f_m\Delta\tau_{az}+\frac{f_m}{f_c}\sin\theta_{az}\sin\theta_{el}=2z\ \ ;\ \ z\in\mathbb{Z} \tag{12}$$

The beam-centre expressions have been summarised in (13). The detailed analysis of the different formula cases and the derivation have been provided in Appendix A.

B. Beam width $\Omega(\epsilon,N)$

The spatial occupancy of beams is defined by a continuous angular region $\mathcal{A}_m$ that satisfies the minimum beamforming gain constraint with respect to gain constant ϵ. Mathematically, $\mathcal{A}_m$ can be defined as follows

$$\mathcal{A}_m=\left\{\left(\theta_{az},\theta_{el}\right)\middle|G\left(\theta_{az},\theta_{el},f_m\right)\geq\left(1-\epsilon\right)N_R\right\}. \tag{14}$$

The occupancy can also be defined in the azimuth and elevation by $\mathcal{A}_{az,m}$ and $\mathcal{A}_{el,m}$, respectively. The regions $\mathcal{A}_{az,m}$ and $\mathcal{A}_{el,m}$ are obtained by separately solving the beamforming gain constraints in the two planes with respect to constants ϵ_{az} and ϵ_{el} respectively, and they can be mathematically expressed as follows

$$\mathcal{A}_{az,m}=\left\{\left(\theta_{az},\theta_{el}\right)\middle|G_{az}\left(\theta_{az},\theta_{el},f_m\right)\geq\left(1-\epsilon_{az}\right)N_{az}\right\}, \tag{15}$$

$$\mathcal{A}_{el,m}=\left\{\left(\theta_{az},\theta_{el}\right)\middle|G_{el}\left(\theta_{el},f_m\right)\geq\left(1-\epsilon_{el}\right)N_{el}\right\}. \tag{16}$$

Fig. 3 illustrates the three regions using a beam example. Note that the intersection of the two angular regions in (15)

$$\theta^{\star}_{el,m} = \begin{cases} \cos^{-1}\left[1 - \mathrm{mod}\left(2f_c\Delta\tau_{el} + 1, 2\frac{f_c}{f_m}\right)\right], & \text{if } \frac{f_m}{2f_c} \geq a_{\min} \quad ① \\ \cos^{-1}\left[1 - 2\frac{f_c}{f_m} - \mathrm{mod}\left(2f_c\Delta\tau_{el} + 1, 2\frac{f_c}{f_m}\right)\right], & \text{if } \frac{f_m}{2f_c} \geq a_{\max} \quad ② \\ \text{No solution}, & \text{if } \frac{f_m}{2f_c} < a_{\min} \quad ③ \end{cases}$$

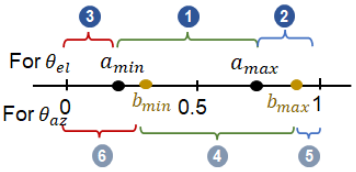

$$\theta^{\star}_{az,m} = \begin{cases} \sin^{-1}\left[1 - \mathrm{mod}\left(\frac{2f_c\Delta\tau_{az}}{\sin\theta^{\star}_{el,m}} + 1, 2\frac{f_c}{f_m}\frac{1}{\sin\theta^{\star}_{el,m}}\right)\right], & \text{if } \frac{f_m}{2f_c} \geq b_{\min} \quad ④ \\ \sin^{-1}\left[1 - 2\frac{f_c}{f_m\sin\theta^{\star}_{el,m}} - \mathrm{mod}\left(\frac{2f_c\Delta\tau_{az}}{\sin\theta^{\star}_{el,m}} + 1, 2\frac{f_c}{f_m}\frac{1}{\sin\theta^{\star}_{el,m}}\right)\right], & \text{if } \frac{f_m}{2f_c} \geq b_{\max} \quad ⑤ \\ \text{No solution}, & \text{if } \frac{f_m}{2f_c} < b_{\min} \quad ⑥ \end{cases} \tag{13}$$

$$a_{\min} = \min\left\{1 - \mathrm{mod}\left(f_m\Delta\tau_{el}, 1\right), \mathrm{mod}\left(f_m\Delta\tau_{el}, 1\right)\right\} \quad ; \quad b_{\min} = \min\left\{1 - \mathrm{mod}\left(f_m\Delta\tau_{az}, 1\right), \mathrm{mod}\left(f_m\Delta\tau_{az}, 1\right)\right\}$$
$$a_{\max} = \max\left\{1 - \mathrm{mod}\left(f_m\Delta\tau_{el}, 1\right), \mathrm{mod}\left(f_m\Delta\tau_{el}, 1\right)\right\} \quad ; \quad b_{\max} = \max\left\{1 - \mathrm{mod}\left(f_m\Delta\tau_{az}, 1\right), \mathrm{mod}\left(f_m\Delta\tau_{az}, 1\right)\right\}$$

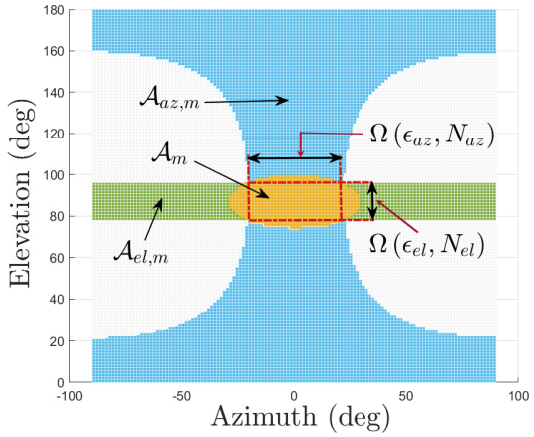

Fig. 3: Angular regions $\mathcal{A}_{az,m}$, $\mathcal{A}_{el,m}$ and $\mathcal{A}_m$ satisfying azimuth and elevation beamforming gain constraints (15) (16), and overall beamforming gain constraint (14) respectively. Here, $N_{az} = 2$, $N_{el} = 4$, $\epsilon = 0.5$, $\epsilon_{az} = \epsilon_{el} = 1 - \sqrt{1-\epsilon} = 0.2929$.

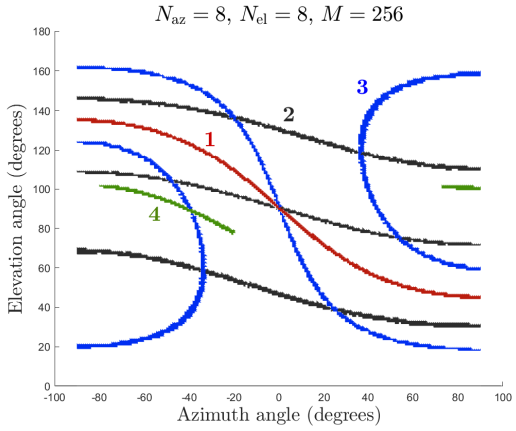

Fig. 4: Trajectory of beam-centres of all beams for different values of K. **1.** $K = 1$, $\Delta\tau_{el} = \frac{1}{BW}$. **2.** $K = 3$, $\Delta\tau_{el} = \frac{1}{BW}$. **3.** $K = 1/3$, $\Delta\tau_{el} = \frac{3}{BW}$. **4.** $\Delta\tau_{el} = \frac{1}{5BW}$, $\Delta\tau_{az} = \frac{1}{8BW}$.

and (16), denoted by a red dotted rectangle in Fig. 3, roughly coincides with the elliptical region $\mathcal{A}_m$. In fact, when the condition $(1-\epsilon_{az})(1-\epsilon_{el}) \geq (1-\epsilon)$ is satisfied, the rectangle is inscribed in $\mathcal{A}_m$. The beam widths $\Omega(\epsilon_{az}, N_{az})$ and $\Omega(\epsilon_{el}, N_{el})$ can be inferred from the dimensions (angular span) of the dotted rectangle along the azimuth and elevation planes, respectively. The beam width is inversely proportional to the number of antennas in the respective plane, i.e., $\Omega(\epsilon, N) \propto 1/N$. $\Omega(0.5, N) = \frac{0.886}{N}$, $\Omega\left(\frac{1}{\sqrt{2}}, N\right) = \frac{0.63784}{N}$ [12, Chapt 22.7].

C. Choice of $\Delta\tau_{az}$ and $\Delta\tau_{el}$

The choice of delay tap spacings $\Delta\tau_{az}$ and $\Delta\tau_{el}$ determines the angular separation between consecutive beams along the azimuth and elevation planes, thereby impacting the frequency-spatial spread of the beams across the 3D angular region. The ratio $K = \Delta\tau_{az}/\Delta\tau_{el}$ governs the relative angular separation between consecutive beams in the azimuth and elevation planes, and in an intuitive sense, defines the local slope of beam trajectory in the region $\theta_{az} \to 0, \theta_{el} \to \pi/2$.

$$\lim_{\substack{\theta_{az}\to 0 \\ \theta_{el}\to \pi/2}} \left(\frac{\Delta\theta_{el}}{\Delta\theta_{az}}\right) \approx \frac{1}{K} \tag{17}$$

Our previous work on linear TTD arrays with uniform delay spacing $\Delta\tau$ showed that beam-spread over the entire angular range along the plane could only be achieved if $\Delta\tau \geq (1/BW)$ [13]. To ensure beam-spread over the entire azimuth and elevation angular ranges ($[-\pi/2, \pi/2]$ and $[0, \pi]$ respectively), the planar TTD array delay spacings must satisfy $\Delta\tau_{el} \geq 1/BW$ and $\Delta\tau_{az} \geq 1/BW$. With $K < 1$, or equivalently $\Delta\tau_{az} < \Delta\tau_{el}$, consecutive beams exhibit greater angular separation along the elevation than along the azimuth, which leads to multiple steep sloped (near-vertical) beam trajectories, as seen in Fig. 4 and Fig. 5(b). On the other hand, when $K > 1$, or equivalently $\Delta\tau_{az} > \Delta\tau_{el}$, consecutive beams experience greater angular separation along the azimuth than along the elevation, resulting in K horizontally oriented beam trajectories. As K increases, the spherical coverage efficiency of the beams improves, as is

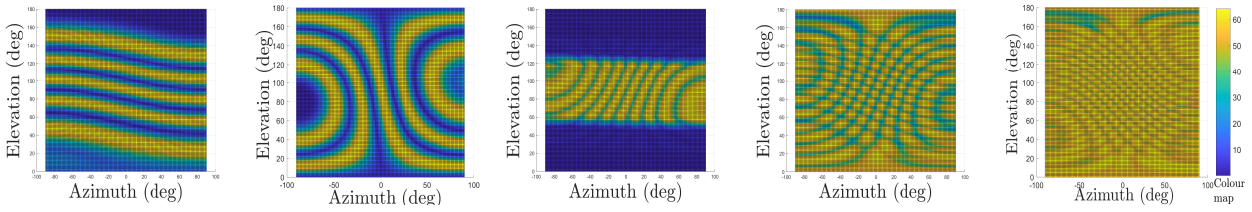

(a) (b) (c) (d) (e)

Fig. 5: The total beam scan patterns of all subcarriers plotted on a 128×128 azimuth-elevation angle grid. The color map denotes the beamforming gain. $N_{az} = N_{el} = 8$, $f_c = 60GHz$, $BW = 6GHz$, $K_{opt} = 26$, $M = 128$ unless stated otherwise. **(a)** $\Delta\tau_{el} = \frac{1}{BW}$, $\Delta\tau_{az} = \frac{5}{BW}$, $K = 5$, $\eta_{cov} = 46.4\%$. **(b)** $\Delta\tau_{el} = \frac{5}{BW}$, $\Delta\tau_{az} = \frac{1}{BW}$, $K = \frac{1}{5}$, $\eta_{cov} = 52.3\%$. **(c)** $\Delta\tau_{el} = \frac{1}{2BW}$, $\Delta\tau_{az} = \frac{26}{BW}$, $K = 26$, $\eta_{cov} = 37.1\%$. **(d)** $\Delta\tau_{el} = \frac{1}{BW}$, $\Delta\tau_{az} = \frac{26}{BW}$, $K = 26$, $M = 128$, $\eta_{cov} = 93.62\%$. **(e)** $\Delta\tau_{el} = \frac{1}{BW}$, $\Delta\tau_{az} = \frac{26}{BW}$, $K = 26$, $M = 256$, $\eta_{cov} = 99.9\%$.

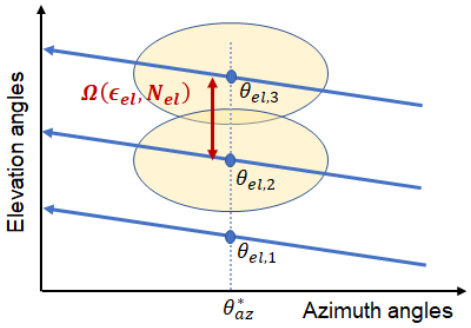

Fig. 6: Constrain elevation angle separation between adjacent trajectories along a chosen θ^*_{az}.

seen in Fig. 5

The above discussion clearly establishes that optimising the ratio $K = \Delta\tau_{az}/\Delta\tau_{el}$ is the first step towards achieving beams with full spherical coverage. In this paper, we focus on the case where $K > 1$ or $\Delta\tau_{az} > \Delta\tau_{el}$. There are K horizontally oriented beam trajectories. We fix an arbitrary θ^*_{az}, and consider the beam-centres from each of the K trajectories lying along the chosen azimuth angle. The intuition here is to fix $\Delta\tau_{el} = 1/BW$ and determine the smallest value of $\Delta\tau_{az} = K/BW$ such that the elevation angle separation between adjacent beam-trajectories is smaller than the elevation beam-width $\Omega(\epsilon_{el}, N_{el})$ for any given azimuth angle θ^*_{az}, as illustrated in Fig. 6. Mathematically, this can be expressed as follows

$$\min_{m_1,m_2} \left|\theta_{el,m_1|\theta^*_{az}} - \theta_{el,m_2|\theta^*_{az}}\right| \leq \Omega(\epsilon_{el}, N_{el}) \qquad (18)$$

The above condition ensures that the beams of two adjacent trajectories are *close enough*, such that no additional beams can be accommodated between them without spatial overlap.

Ignoring the beam squint effect, i.e., assuming $f_m/f_c \approx 1$, the associated pointing direction angle pairs along a fixed azimuth angle θ^*_{az} satisfy the following conditions

$$\begin{aligned} &\frac{2f_m K}{BW} + \sin(\theta_{el,m})\sin(\theta^*_{az}) = 2z_1 \\ &\frac{2f_m}{BW} + \cos(\theta_{el,m}) = 2z_2 \quad , \quad z_1, z_2 \in \mathbb{Z} \end{aligned} \qquad (19)$$

Combining the equations in (19), we get the following

$$\begin{aligned} &A\cos\left(\theta_{el,m} + \hat{\phi}\right) = 2(Kz_2 - z_1) \\ \implies \quad &\theta_{el,m} = 2n\pi \pm \cos^{-1}\left(\frac{2}{A}(Kz_2 - z_1)\right) - \hat{\phi} \end{aligned} \qquad (20)$$

where $A = \sqrt{K^2 + \sin^2(\theta^*_{az})}$ and $\hat{\phi} = \tan^{-1}(\sin(\theta^*_{az})/K)$. It can be shown that as K increases, the elevation angle separation between beams along a fixed azimuth angle decreases. By solving (18) and (20) for the set of subcarriers mapped to the region $(0 \pm \Delta\theta_{az}, \pi/2 \pm \Delta\theta_{el})$, where $\Delta\theta_{az} \to 0, \Delta\theta_{el} \to 0$, we obtain the optimal ratio $K \geq 2/\Omega(\epsilon_{el}, N_{el})$. For example, with $\epsilon_{el} = 1/\sqrt{2}$, $K \approx 2N_{el} \times 1.56$. Therefore, choosing the spacings $\Delta\tau_{az}$ and $\Delta\tau_{el}$ as

$$\Delta\tau_{az} \geq \frac{K}{BW}, \quad \Delta\tau_{el} \geq \frac{1}{BW}, \quad K \geq \frac{2}{\Omega(\epsilon_{el}, N_{el})}, \qquad (21)$$

ensures sufficient beam proximity along the elevation, and the coverage of the entire azimuth and elevation angle ranges. The maximum delay range required is therefore $(N_{\text{az}} - 1)\Delta\tau_{\text{az}} + (N_{\text{el}} - 1)\Delta\tau_{\text{el}}$.

D. Optimal number of subcarriers M

Constraining beam separation along the elevation by optimally selecting the delay spacings in accordance with (21) alone is not enough to achieve full spherical coverage. We also need to ensure beam proximity along the azimuth plane. For a given set of array parameters, fixing the ratio of the delay spacings K sets the trajectory that beams can follow, and in turn, the beam separation along the elevation. How *closely packed* the beams are along these trajectories now depends on the number of subcarriers used for the codebook. As can be easily verified from the expressions in (13), increasing the number of subcarriers used, while keeping all array parameters fixed, results in more closely spaced beams. In other words, the beam separation along the azimuth decreases as the number of subcarriers increases. Our objective is to determine the lower bound on the number of subcarriers for which the azimuth angle separation between adjacent beams along a given elevation angle θ^*_{el} is smaller than the beam width in the azimuth $\Omega(\epsilon_{az}, N_{az})$, as illustrated in Fig. 7. This is expressed

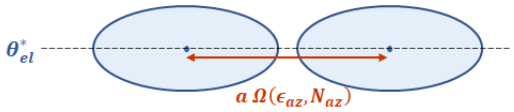

Fig. 7: Constrain adjacent beam separation in the azimuth plane along a chosen θ^*_{el}.

as follows

$$\min_{j,\ \text{given}\ \theta^*_{el}} |\theta_{az,j} - \theta_{az,j+1}| \leq a\Omega\left(\epsilon_{az}, N_{az}\right). \tag{22}$$

Here, $a \geq 1$ is a relaxation constant, representing the extent of relaxation in the azimuth beam-proximity constraint in (22). $(a = 1)$ indicates strict proximity and can be visualised by perfectly touching ellipses in Fig. 7. Upon finding the pointing directions of consecutive beams along a given θ^*_{el} and accounting for the constraint in (22), the lower bound on the number of subcarriers needed to achieve full coverage can be given as follows

$$M \geq \frac{4}{a} \frac{BW\Delta\tau_{el}}{\Omega\left(\epsilon_{az}, N_{az}\right)\Omega\left(\epsilon_{el}, N_{el}\right)} \tag{23}$$

The complete derivation of (23) is provided in Appendix B.

The 3D rainbow beam codebook designed in accordance with (21) and (23) can be shown to achieve 100% spherical coverage based on (10). This completes the 3D rainbow beam codebook design problem.

IV. 3D Beam Training Algorithm

This section proposes a power-based beam training algorithm that leverages the 3D rainbow beam codebook designed in Sec. III.

The designed codebook ensures that different angular directions are probed with different OFDM subcarriers. Thus, information of the AoA associated with the dominant propagation direction is embedded in the signal spectrum. Due to the deterministic frequency-spatial mapping described in (13), the AoA angle pair $(\hat{\theta}_{\text{az}}, \hat{\theta}_{\text{el}})$ can be estimated by identifying the subcarrier with the highest received signal power. The signal power $\hat{p}[m]$ at the m-th subcarrier can be computed as $\hat{p}[m] = |Y[m]|^2$. Assuming that m^* is the index of the subcarrier with the highest power, the beam training algorithm can be summarized as follows

$$(\hat{\theta}_{\text{az}}, \hat{\theta}_{\text{el}}) = (\theta_{az,m^*}, \theta_{el,m^*}), \quad \text{where} \quad m^* = \arg\max_m |Y[m]|^2 \tag{24}$$

Since this is a lookup table based approach, the AoA estimation accuracy is limited by the number of angular directions that are probed in the azimuth and elevation. With M subcarriers used for beam training, the complexity of the algorithm in (24) scales as $\mathcal{O}(M)$.

V. Simulation Results

This section presents simulation results to illustrate the performance of the beam training algorithm.

The simulation utilizes QuaDRiGa simulator [14] with mmMAGIC 28GHz channel model [15] in urban micro (UMi)

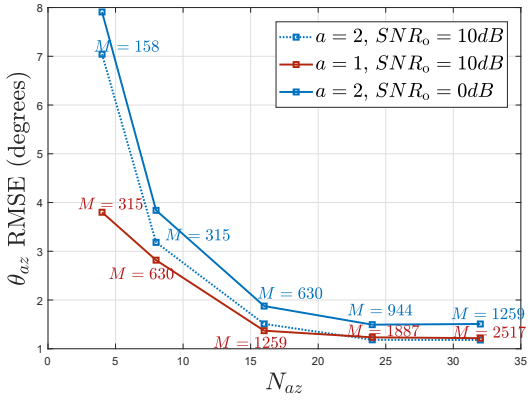

Fig. 8: AoA estimation RMSE for θ_{az} against azimuth array dimension N_{az}, with constant $N_{el} = 8$ antennas.

line-of-sight (LoS) environment. We consider the carrier frequency f_{c} =60 GHz, bandwidth 400 MHz, and receiver antenna array with $N_{el} = 8$ antennas along the elevation plane, whereas N_{az} is variable. We choose gain constants $\epsilon = 0.5$, $\epsilon_{az} = \epsilon_{el} = 1/\sqrt{2}$. The delay tap spacings $\Delta\tau_{el} = 1/BW$ =2.5 ns, $\Delta\tau_{\text{az}} = 2/\Omega\left(\epsilon_{el}, N_{el}\right)$ =65 ns. The number of subcarriers is $M = 4\left(20 \times N_{az}\right)/a$, where $a \geq 1$ represents a relaxation in (22). Each array geometry investigated achieves $\eta_{cov} = 100\%$ for the array parameters considered.

Fig. 8 presents the root mean square error (RMSE) of the estimated azimuth angle against the number of azimuth antennas N_{az}. The performance is evaluated for two different values of base signal-to-noise ratio (SNR), including $SNR_{\text{o}} = 0\ dB$ and $SNR_{\text{o}} = 10\ dB$[1].As expected, the azimuth angle estimation RMSE is seen to decrease as the number of azimuth antennas N_{az} increases. Larger arrays have narrower beams since $\Omega(\epsilon_{az}, N_{az}) \propto \frac{1}{N_{az}}$, which in turn improves the estimation accuracy of the azimuth AoA.

Increasing SNR_{o} from 0 dB to 10 dB results in a decreased RMSE for $\hat{\theta}_{az}$ for all N_{az}. Further, a codebook with the optimal number of subcarriers ($a = 1$, no relaxation) performs significantly better than the relaxed codebook ($a = 2$) for smaller array sizes. However, as N_{az} increases beyond 16 antennas, the strict codebook achieves comparable estimation RMSE to the relaxed codebook at the same SNR. This suggests that codebook relaxations can achieve reasonably good estimation accuracy for large arrays, thereby hinting at a trade-off that could be exploited to reduce the codebook size,

[1]As the array dimension along the azimuth increases, the number of needed subcarriers M increases. In order to maintain a constant SNR per subcarrier, we increase the total transmit power as the array size increases. This, however, increases the total SNR. The base SNR for the smallest array size being studied ($N_{az} = 4, N_{el} = 8$) is denoted by SNR_{o}. The total received SNR varies with the number of azimuth antennas as follows

$$SNR_{N_{az_2}} = SNR_{N_{az_1}} + 10\log_{10}\left(M_{N_{az_2}}/M_{N_{az_1}}\right)$$

to ensure a constant SNR per subcarrier. Thus, the transmit power adjustment term of $\log_{10}\left(M_{N_{az_2}}/M_{N_{az_1}}\right)$ is needed when the azimuth array size is increased from N_{az_1} to N_{az_2}.

algorithm complexity, and power consumption, depending on the array size.

VI. Conclusions and Future works

In this work, we present the design of 3D Rainbow beam codebook using a TTD planar array for fast beam training in wideband millimeter wave systems. With a dedicated delay network along the azimuth and elevation planes, it is possible to realise frequency dependent beams spanning the entire 3D angular space with a single OFDM symbol. We obtained the frequency-spatial relation of the 3D codebook beams by deriving mathematical expressions for beam-centres as a function of TTD planar array parameters and subcarrier frequency, thereby establishing that the beam-coverage depends on the design of delay taps and the number of subcarriers used in the codebook. We then derived the optimal delay spacings along the azimuth and elevation planes, and the number of subcarriers needed, to construct a 3D beam codebook that achieves full spherical coverage across the 3D hemisphere. Based on this codebook, a single-shot power-based beam training algorithm is proposed. Simulation results show that the AoA estimation accuracy depends on the array geometry and codebook design.

VII. Acknowledgement

This work was supported in part by the NSF under grant 1955672. This work was also supported in part by the ComSenTer and CONIX Research Centers, two of six centers in JUMP, a Semiconductor Research Corporation (SRC) program sponsored by DARPA.

Appendix A
Derivation of beam-centres in (13)

Beam-centres $\left\{\theta^{\star}_{\text{az},m}, \theta^{\star}_{\text{el},m}\right\}$ are the angle pair that achieve the maximum beamforming gain N_R.

$$\left\{\theta^{\star}_{\text{az},m}, \theta^{\star}_{\text{el},m}\right\} = \left\{ (\theta_{az}, \theta_{el}) \,\middle|\, G(\theta_{az}, \theta_{el}, f_m) = N_R \right\} \quad (25)$$

$$\implies G_{\text{az}}\left(\theta^{\star}_{\text{az},m}, \theta^{\star}_{\text{el},m}, f_m\right) = N_{\text{az}} \;;\; G_{\text{el}}\left(\theta^{\star}_{\text{el},m}, f_m\right) = N_{\text{el}}$$

As discussed in Sec. III-A, we first solve for $\theta^{*}_{el,m}$. By L'Hospital rule, $G_{\text{el}}(\Psi_{\text{el}}) = N_{el}$ when $\Psi_{\text{el}} = 0$, since $\lim_{\Psi_{\text{el}} \to 0} \left| \frac{\sin\left[N_{el}\frac{\pi}{2}\Psi_{el}\right]}{\sin\left[\frac{\pi}{2}\Psi_{el}\right]} \right|^2 = N_{el}^2$. The elevation beam-centre angle can be obtained by solving (11). We first find the permissible values of $z \in \mathbb{Z}$ so as to satisfy the range of the cosine function: $\cos(\theta_{\text{el}}) = 2(f_c/f_m)(z - f_m\Delta\tau_{el}) \in [-1, 1]$ as shown below.

$$f_m\Delta\tau_{el} - \frac{1}{2}\frac{f_m}{f_c} \le z \le f_m\Delta\tau_{el} + \frac{1}{2}\frac{f_m}{f_c} \;\;;\;\; z \in \mathbb{Z} \quad (26)$$

We then substitute these integer values of z back into (11) to obtain $\theta^{\star}_{\text{el},m}$. It is clear from (26) that z lies in an interval of length f_m/f_c. If $(f_m/f_c) < 1$, then z has a solution if the interval contains an integer. If $(f_m/f_c) \ge 1$, then z can have one or two solutions depending on the number of integers in the interval. This gives rise to three cases.

Case 1: No solution. This happens only when $(f_m/f_c) < 1$, and the permissible range of z does not contain any integer. This condition can be mathematically represented by the following inequalities.

$$\begin{aligned} \lfloor f_m\Delta\tau_{el} \rfloor &\le f_m\Delta\tau_{el} - \frac{1}{2}\frac{f_m}{f_c} \\ \implies \frac{1}{2}\frac{f_m}{f_c} &\le \text{mod}\,(f_m\Delta\tau_{el}, 1) \end{aligned} \quad (27)$$

$$\begin{aligned} \lfloor f_m\Delta\tau_{el} \rfloor + 1 &\ge f_m\Delta\tau_{el} + \frac{1}{2}\frac{f_m}{f_c} \\ \implies \frac{1}{2}\frac{f_m}{f_c} &\le 1 - \text{mod}\,(f_m\Delta\tau_{el}, 1) \end{aligned} \quad (28)$$

Note that $\lfloor b_o \rfloor = b_o - \text{mod}\,(b_o, 1)$. Equations (27) and (28) imply that there is no integer solution z that satisfies (11). Consequently, $\theta^{\star}_{\text{el},m}$ has no solution. Physically, this means that subcarriers satisfying (27) and (28) do not achieve maximum elevation gain $= N_{el}$, and in turn, maximum beamforming gain $= N_R$, at any θ_{el}. Equations (27) and (28) can be summarised as:

$$\boxed{\begin{aligned} &\frac{1}{2}\frac{f_m}{f_c} < \min\left\{\text{mod}\,(f_m\Delta\tau_{el}, 1), 1 - \text{mod}\,(f_m\Delta\tau_{el}, 1)\right\} \\ &\implies \theta^{*}_{\text{el},m} \;:\; \text{no solution} \end{aligned}}$$

Case 2: One solution. The interval of length (f_m/f_c) contains exactly one integer. Here, we consider two sub-cases depending on the relative position of this integer, say z_{o}, with respect to $f_m\Delta\tau_{el}$.

i Integer $z_{\text{o}} \in [f_m\Delta\tau_{el} - (f_m/2f_c), f_m\Delta\tau_{el})$:
This can be captured using the condition $\lfloor f_m\Delta\tau_{el} \rfloor \ge f_m\Delta\tau_{el} - (f_m/2f_c)$, which simplifies to $\frac{1}{2}\frac{f_m}{f_c} \ge \text{mod}\,(f_m\Delta\tau_{el}, 1)$. The condition $\lfloor f_m\Delta\tau_{el} \rfloor + 1 \ge f_m\Delta\tau_{el} + (f_m/2f_c)$ further enforces the presence of a single integer solution, which upon simplification yields $\frac{1}{2}\frac{f_m}{f_c} \le 1 - \text{mod}\,(f_m\Delta\tau_{el}, 1)$. Thus, z has one solution when f_m satisfies $\frac{1}{2}\frac{f_m}{f_c} \in [\text{mod}\,(f_m\Delta\tau_{el}, 1), 1 - \text{mod}\,(f_m\Delta\tau_{el}, 1))$, for $\text{mod}\,(f_m\Delta\tau_{el}, 1) < 1 - \text{mod}\,(f_m\Delta\tau_{el}, 1)$.

ii Integer $z_{\text{o}} \in [f_m\Delta\tau_{el}, f_m\Delta\tau_{el} + (f_m/2f_c))$:
This can be captured using the conditions $\lfloor f_m\Delta\tau_{el} \rfloor + 1 \le f_m\Delta\tau_{el} + (f_m/2f_c)$ and $\lfloor f_m\Delta\tau_{el} \rfloor \ge f_m\Delta\tau_{el} - (f_m/2f_c)$, which simplify to $\frac{1}{2}\frac{f_m}{f_c} \ge 1 - \text{mod}\,(f_m\Delta\tau_{el}, 1)$ and $\frac{1}{2}\frac{f_m}{f_c} \le \text{mod}\,(f_m\Delta\tau_{el}, 1)$ respectively. Thus, the range of frequencies for which z has one solution is given by $\frac{1}{2}\frac{f_m}{f_c} \in [1 - \text{mod}\,(f_m\Delta\tau_{el}, 1), \text{mod}\,(f_m\Delta\tau_{el}, 1))$ when $\text{mod}\,(f_m\Delta\tau_{el}, 1) \ge 1 - \text{mod}\,(f_m\Delta\tau_{el}, 1)$.

Upon combining the mutually exclusive cases (i) and (ii), we summarize the condition on $(f_m/2f_c)$ for single solution, as shown below. The integer z takes the value $\lfloor f_m\Delta\tau_{el} + (f_m/2f_c) \rfloor$, which upon substitution in (11), yields $\theta^{\star}_{\text{az},m}$.

$$\boxed{\begin{aligned} &\min\left\{\text{mod}\,(f_m\Delta\tau_{el}, 1), 1 - \text{mod}\,(f_m\Delta\tau_{el}, 1)\right\} \le \\ &\quad \frac{1}{2}\frac{f_m}{f_c} < \max\left\{\text{mod}\,(f_m\Delta\tau_{el}, 1), 1 - \text{mod}\,(f_m\Delta\tau_{el}, 1)\right\} \\ &\quad \implies \theta^{\star}_{\text{el},m} = \cos^{-1}\left[1 - \text{mod}\left(2f_c\Delta\tau_{el} + 1, 2\frac{f_c}{f_m}\right)\right] \end{aligned}}$$

Case 3: Two solutions– This happens when $(f_m/f_c) > 1$. The two solutions are $z_1 = \lfloor f_m\Delta\tau_{el} + (f_m/2f_c)\rfloor$ and $z_2 = \lfloor f_m\Delta\tau_{el} + (f_m/2f_c)\rfloor - 1$. The conditions ascertaining two solutions are $\lfloor f_m\Delta\tau_{el}\rfloor \geq f_m\Delta\tau_{el} - (f_m/2f_c)$ and $\lfloor f_m\Delta\tau_{el}\rfloor + 1 \leq f_m\Delta\tau_{el} + (f_m/2f_c)$, which simplify to $\frac{1}{2}\frac{f_m}{f_c} \geq \text{mod}\,(f_m\Delta\tau_{el}, 1)$ and $\frac{1}{2}\frac{f_m}{f_c} \geq 1 - \text{mod}\,(f_m\Delta\tau_{el}, 1)$ respectively, resulting in the following.

$$\frac{1}{2}\frac{f_m}{f_c} \geq \max\left\{\text{mod}\,(f_m\Delta\tau_{el}, 1), 1 - \text{mod}\,(f_m\Delta\tau_{el}, 1)\right\}$$
$$\implies \theta^{\star}_{\text{el},m_1} = \cos^{-1}\left[1 - \text{mod}\left(2f_c\Delta\tau_{el} + 1, 2\frac{f_c}{f_m}\right)\right]$$
$$\theta^{\star}_{\text{el},m_2} = \cos^{-1}\left[1 - 2\frac{f_c}{f_m} - \text{mod}\left(2f_c\Delta\tau_{el} + 1, 2\frac{f_c}{f_m}\right)\right]$$

Having found $\theta^{\star}_{\text{el},m}$, the azimuth beam-centre angle can be determined as $\theta^{\star}_{\text{az},m} = \left\{\theta_{az}\middle| G\left(\theta_{az}, \theta^{\star}_{\text{el},m}, f_m\right) = N_{\text{az}}\right\}$. We compute $\theta^{\star}_{\text{az},m}$ by solving (12) in a similar manner as we did for $\theta^{\star}_{\text{el},m}$. The permissible range of z is now given by $f_m\Delta\tau_{el} - \sin\theta^{\star}_{\text{el},m}\,(f_m/2f_c) \leq z \leq f_m\Delta\tau_{el} + \sin\theta^{\star}_{\text{el},m}\,(f_m/2f_c)$; $z \in \mathbb{Z}$. We set up three cases: for no solution, one solution and two solutions in the same manner as we did for the elevation beam-centre, and thereby obtain the expressions for $\theta^{\star}_{\text{az},m}$ as given in (13).

Appendix B
Derivation of optimal ratio $K = \Delta\tau_{az}/\Delta\tau_{el}$

The analysis in Sec. III-C restricts attention to subcarriers with frequency close to f_c, i.e., assuming $f_m/f_c \approx 1$. Combining the equations in (19), we get the following

$$K\,(2z_2 - \cos(\theta_{el,m})) + \sin(\theta_{el,m})\sin(\theta^*_{az}) = 2z_1$$
$$\implies (\sin(\theta_{el,m})\sin(\theta^*_{az}) - K\cos(\theta_{el,m})) = 2Kz_2 - 2z_1$$
$$\implies \text{A}\cos\left(\theta_{el,m} + \phi\right) = 2\left(Kz_2 - 2z_1\right)$$
$$\implies \theta_{el,m} = 2n\pi \pm \cos^{-1}\left(\frac{2}{A}(Kz_2 - z_1)\right) - \hat{\phi}$$

where $\text{A} = \sqrt{\sin^2\theta^*_{az} + K^2}$ and $\phi = \tan^{-1}(\sin(\theta^*_{az})/K)$. The first order approximation of the Taylor series of $\cos^{-1}x$ gives us $\theta_{el,m} = 2n\pi \pm \left(\frac{\pi}{2} - \frac{2}{A}(Kz_2 - z_1)\right) - \hat{\phi}$. Thus, the minimum elevation-angle separation between adjacent horizontal trajectories is given by $\frac{2}{A} \approx \frac{2}{K}$. Solving the constraint in (18) gives us $\frac{2}{K} \leq \Omega(\epsilon_{el}, N_{el})$, which upon further simplification, yields the optimal ratio K described in (21).

Appendix C
Derivation of number of needed subcarriers M

Consider adjacent beams centred at frequencies f_{m1} and f_{m2}, along the elevation angle θ^*_{el}. Assuming $f_m/f_c \approx 1$ and $\theta^*_{\text{el}} \to \pi/2$, we compute the azimuth angle separation between their beam-centres as follows:

$$2f_m\Delta\tau_{\text{az}} + \sin(\theta_{\text{az},m})\sin(\theta^*_{\text{el}}) = 2z \;\; ; \;\; z \in \mathbb{Z}$$
$$\implies \sin(\theta_{\text{az},m}) = \frac{2}{\sin\theta^*_{\text{el}}}\left(z - f_m\Delta\tau_{az}\right)$$
$$\implies \theta_{\text{az},m} = \sin^{-1}\left(\frac{2}{\sin(\theta^*_{\text{el}})}\left(z - f_m\Delta\tau_{az}\right)\right)$$
$$\approx 2z - 2f_m\Delta\tau_{az}$$

This follows from the first order approximation of Taylor series expansion of $\sin^{-1}(x)$, and $\lim_{\theta\to\frac{\pi}{2}}\sin\theta = 1$. The azimuth angle separation $|\theta_{\text{az},m_1} - \theta_{\text{az},m_2}|$ can thus be approximated as $2|f_{m1} - f_{m2}|\Delta\tau_{az}$. Since $|f_{m1} - f_{m2}| = \frac{BW}{M}$, the azimuth angle separation becomes $2 \times \frac{BW}{M}\Delta\tau_{az}$. Upon substitution in (22), we get $2 \times \frac{BW}{M}\Delta\tau_{az} \leq a\Omega\left(\epsilon_{az}, N_{az}\right)$ $\implies M \geq \frac{2}{a}\frac{BW\times\Delta\tau_{az}}{\Omega(\epsilon_{az}, N_{az})}$. Adhering to the optimal K described in (21) gives us the lower bound on M obtained in (23).

References

[1] V. Boljanovic, H. Yan, C.-C. Lin, S. Mohapatra, D. Heo, S. Gupta, and D. Cabric, "Fast beam training with true-time-delay arrays in wideband millimeter-wave systems," *IEEE Transactions on Circuits and Systems I: Regular Papers*, vol. 68, no. 4, pp. 1727–1739, 2021.

[2] Y. Ghasempour, C.-Y. Yeh, R. Shrestha, D. Mittleman, and E. Knightly, "Single shot single antenna path discovery in thz networks," in *Proceedings of the 26th Annual International Conference on Mobile Computing and Networking*, ser. MobiCom '20. New York, NY, USA: Association for Computing Machinery, 2020. [Online]. Available: https://doi.org/10.1145/3372224.3380895

[3] C.-C. Lin, C. Puglisi, E. Ghaderi, S. Mohapatra, D. Heo, S. Gupta, H. Yan, V. Boljanovic, and D. Cabric, "A 4-element 800mhz-bw 29mw true-time-delay spatial signal processor enabling fast beam-training with data communications," in *ESSCIRC 2021 - IEEE 47th European Solid State Circuits Conference (ESSCIRC)*, 2021, pp. 287–290.

[4] H. Saeidi, S. Venkatesh, X. Lu, and K. Sengupta, "22.1 thz prism: One-shot simultaneous multi-node angular localization using spectrum-to-space mapping with 360-to-400ghz broadband transceiver and dual-port integrated leaky-wave antennas," in *2021 IEEE International Solid- State Circuits Conference (ISSCC)*, vol. 64, 2021, pp. 314–316.

[5] R. Li, H. Yan, and D. Cabric, "Rainbow-link: Beam-alignment-free and grant-free mmW multiple access using true-time-delay array," 2021. [Online]. Available: https://arxiv.org/abs/2109.04357

[6] Y. Ghasempour, C.-Y. Yeh, R. Shrestha, Y. Amarasinghe, D. Mittleman, and E. W. Knightly, "Leakytrack: Non-coherent single-antenna nodal and environmental mobility tracking with a leaky-wave antenna," in *Proceedings of the 18th Conference on Embedded Networked Sensor Systems*, ser. SenSys '20. New York, NY, USA: Association for Computing Machinery, 2020, p. 56–68. [Online]. Available: https://doi.org/10.1145/3384419.3430717

[7] J. Tan and L. Dai, "Wideband beam tracking in THz massive MIMO systems," *IEEE Journal on Selected Areas in Communications*, vol. 39, no. 6, pp. 1693–1710, 2021.

[8] J. Mo, B. L. Ng, S. Chang, P. Huang, M. N. Kulkarni, A. Alammouri, J. C. Zhang, J. Lee, and W.-J. Choi, "Beam codebook design for 5g mmwave terminals," *IEEE Access*, vol. 7, pp. 98 387–98 404, 2019.

[9] J. Yang, W. Ryoo, W. Sung, J.-H. Kim, and J. Park, "3d antenna structures using uniform triangular arrays for efficient full-directional multiuser transmission," *International Journal of Antennas and Propagation*, vol. 2019, pp. 1–12, 11 2019.

[10] W. Wu, D. Liu, Z. Li, X. Hou, and M. Liu, "Two-stage 3d codebook design and beam training for millimeter-wave massive mimo systems," in *2017 IEEE 85th Vehicular Technology Conference (VTC Spring)*, 2017, pp. 1–7.

[11] D. Tse and P. Viswanath, *Fundamentals of wireless communication*. Cambridge university press, 2005.

[12] S. J. Orfinidas, *Electromagnetic Waves and Antennas*, (accessed in Dec 1, 2019). [Online]. Available: http://eceweb1.rutgers.edu/~orfanidi/ewa/ewa-1up.pdf

[13] H. Yan, V. Boljanovic, and D. Cabric, "Wideband millimeter-wave beam training with true-time-delay array architecture," in *2019 53rd Asilomar Conference on Signals, Systems, and Computers*, 2019, pp. 1447–1452.

[14] S. Jaeckel, L. Raschkowski, K. Börner, and L. Thiele, "QuaDRiGa: A 3-D multi-cell channel model with time evolution for enabling virtual field trials," *IEEE Trans. Antennas Propag.*, vol. 62, no. 6, pp. 3242–3256, Jun. 2014.

[15] 5GPPP, "D2.2 measurement results and final mmMAGIC channel models," *Tech. Rep.*, 2017. [Online]. Available: https://5g-mmmagic.eu/results